Journal of Nano- and Electronic Physics
Vol. **15** No 4, 04008(4pp) (2023)

Журнал нано- та електронної фізики
Том **15** № 4, 04008(4cc) (2023)

Design of Controller for Bidirectional Non-isolated High Gain Converter in EV Application

Anbazhagan Geetha*, R. Sridhar, P. Suresh, S. Usha, T.M. Thamizh Thentral

Department of Electrical and Electronics Engineering, SRM Institute of Science and Technology, Kattankulathur, Chennai - 603203, Tamil Nadu, India

(Received 11 June 2023; revised manuscript received 14 August 2023; published online 30 August 2023)

An interface between a DC supply and an electric vehicle's drive fed by an inverter is a bidirectional DC-DC converter. In this research, a topology for an electric vehicle based on an induction motor that integrates a high voltage gain bidirectional non-isolated DC/DC converter with a three-phase inverter is proposed. This study compares a bidirectional DC to DC converter inverter system controlled by fuzzy logic (FL), and fractional order proportional integral derivative (FOPID). The suggested converter runs in discontinuous-current mode (DCM), with all switches and diodes switching at zero current. It is possible to operate across a wide duty cycle range while maintaining high output voltage gain, low switching stress, minimal switching losses, and high efficiency. The proposed converter's size and weight are decreased so as to support a wide range of duty cycle operations, maintain lower voltage stress on all devices, ensure equal current sharing among inductors, are simple to control, and require a more compact inductor. The converter also uses a constant input current which offers a choice for various applications. MATLAB Simulink is used to construct, model, and simulate open loop system, closed loop FL and FOPID. The results of these simulations are then reported. The investigations show that FOPID controlled DC-DC converter performed better response.

Keywords: Electric vehicle, Controller, DC/DC Converter, Bidirectional, High gain.

DOI: 10.21272/jnep.15(4).04008 PACS number: 88.85.Hj

1. INTRODUCTION

Due to the pollution-free nature and ability to circumvent the problem of fuel depletion, electric vehicle (EV) drive trains are becoming more and more popular in the environmental community [1]. Traditionally, battery strings in series are used to give the high voltage (HV) needed for EV. However, the uneven charging between the strings and variation in the temperature gradient shorten the lifespan of the batteries. Although paralleling a battery string may solve such issues, the output voltage will be reduced [2]. Yet, the presence of coupling transformer's leakage reactance may result in unsafe HV sparks over the operating switches during switching transients, large copper loss, which is not preferable for large voltage varying applications [3, 4]. Bidirectional isolated converters, offer high voltage gain for stepping up and down the voltage by adjusting the transformers turns ratio. Transient switching losses were reduced thanks to the introduction of soft switching strategies in converters [5-7]. On the other side, as there are more operational switches, there are more conduction losses, more complexity, and more expense.

Switched capacitor (SC) power converters can have smaller converter sizes and higher power densities, but larger voltage gains necessitate larger switched capacitor sizes [8]. Conversely, switching inductor (SL) can tolerate high voltage gains regardless of the operating quadrant [3, 9-10]. Therefore, DC-DC converters with substantial voltage gains have attracted the attention of numerous researchers. In this work, a superior bidirectional topology is sought after for a high voltage gain induction motor-based EV drive. It also covers the use of a closed loop controller to a better converter, which enhances the system's dynamic response.

2. PROPOSED SYSTEM

The schematic layout of the typical conventional converter system is depicted in Fig. 1 It uses four passive elements and has a distinctive X-shaped impedance. Effective power conversions can be made between energy source and the load in all possible methods. The main disadvantage, however, is having low total harmonic distortion (THD) and average power conversion rate (APCR) in the reducing duty ratio range.

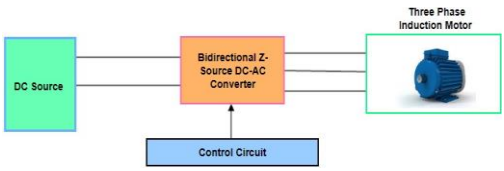

Fig. 1 – Block diagram of the conventional system

The drawback identified from the conventional system can be overcome by the proposed bidirectional DC/DC converter. The proposed system's block diagram is shown in Fig. 2 Both systems are subjected to simulation. The proposed isolated high gain *Z* source system is compared against the non-isolated high voltage gain converter in terms of power handling capacity, voltage boost up capability, and THD.

3. CIRCUIT ANALYSIS

The proposed converter's suggested schematic circuit diagram is shown in Fig. 3 S_1 and S_2 function as semiconductor switches, whilst S_3 and S_4 are active rectifiers. S_1 and S_2 switches are turned on initially. Here, low voltage DC source V_l and the capacitor charges magnetize inductor L_1. The low voltage dc source V_l provides power to the inductor L_2.

* geethaa2@srmist.edu.in
The results were presented at the 3rd International Conference on Innovative Research in Renewable Energy Technologies (IRRET-2023)

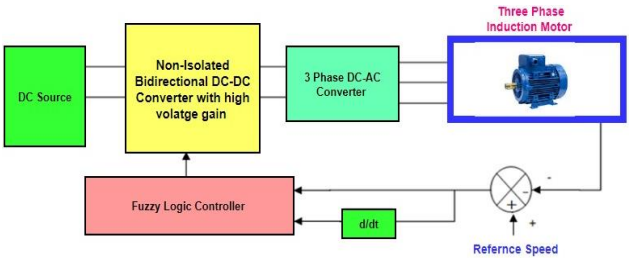

Fig. 2 – Block diagram of the proposed system

The voltages of the L_1 and L_2 inductors are provided in the following equation.

$$\begin{bmatrix} V_{L1inductor} \\ V_{L2inductor} \end{bmatrix} = \begin{bmatrix} 1 & 0 \\ 0 & 0 \end{bmatrix} \begin{bmatrix} V_{capacitor} \\ V_h \end{bmatrix} + \begin{bmatrix} 1 \\ 1 \end{bmatrix} [V_l] \quad (3.1)$$

The S_3 and S_4 switches are on in the following mode, while the S_1 and S_2 switches are off. High voltage output is provided using the L_1 inductor's stored energy and low voltage input V_l. Additionally, the L_2 inductor's stored energy and the low voltage input V_l are used to charge the C capacitor.

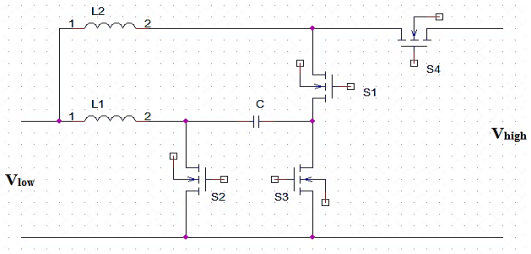

Fig. 3 – Simulation circuit of the proposed system

Under this mode, the voltages between the L_1 and L_2 inductors are as follows.

$$\begin{bmatrix} V_{L1inductor} \\ V_{L2inductor} \end{bmatrix} = \begin{bmatrix} 0 & -1 \\ -1 & 0 \end{bmatrix} \begin{bmatrix} V_{capacitor} \\ V_h \end{bmatrix} + \begin{bmatrix} 1 \\ 1 \end{bmatrix} [V_l] \quad (3.2)$$

Here V_h and V_l are the boosted output and input voltages respectively, $V_{1\text{inductor}}$, $V_{2\text{inductor}}$ and $V_{\text{capacitor}}$ are the inductors and capacitor voltages. $\boldsymbol{\delta}$ denotes the duty ratio.

$$\frac{V_h}{V_l} = \left(\frac{1}{1-\delta}\right)^2 \quad (3.3)$$

The equation for evaluating the inductors rating is

$$L_{1ind} = \frac{\delta(2-\delta)(1-\delta)^2 R_{Load}}{2 * switching\ frequency} \quad (3.4)$$

$$L_{2ind} = \frac{(1-\delta)^4 R_{Load}}{2 * switching\ frequency} \quad (3.5)$$

4. SIMULATION RESULTS

Table 1 displays the simulation results for the proposed and current systems. The comparison shows that the suggested system generates a higher output power while having a lower thd. The speed decreases from 1300 to 1200 rpm for the applied load.

The specified torque is 1.2 nm. The simulation and hardware parameters are listed in below Table 2. To enhance the system's transient properties, a FOPID, and fuzzy controller design was carried out for the boost operation. While FLC relies on human intuition, linear control systems use a minimal transfer function. To determine error, the drive' actual speed is sensed and compared to reference speed. Additionally, the efficiency is much higher than in traditional mode.

Table 1 – Compares analysis of the proposed and existing sy tems

System	Voltage (In)	Voltage (Out)	THD (I)	Power (Out)
Existing	80 V	200 V	12.31 %	2300 W
Proposed	80 V	220 V	7.25 %	3300 W

Table 2 – The values of different components used in simulation and hardware

Parameters	Simulation	Hardware
V_{in}	100 V	24 V
L_1, L_2	10 mH	2.5 mH
C_1	64 μF	2 mH
C_2, C_3	1200 μF	2200 μF
L_3	200 mH	2.2 mH
Semiconductor switch(IRF840)	500 V/8 A	
Uncontrolled switch	230 V/1 A	

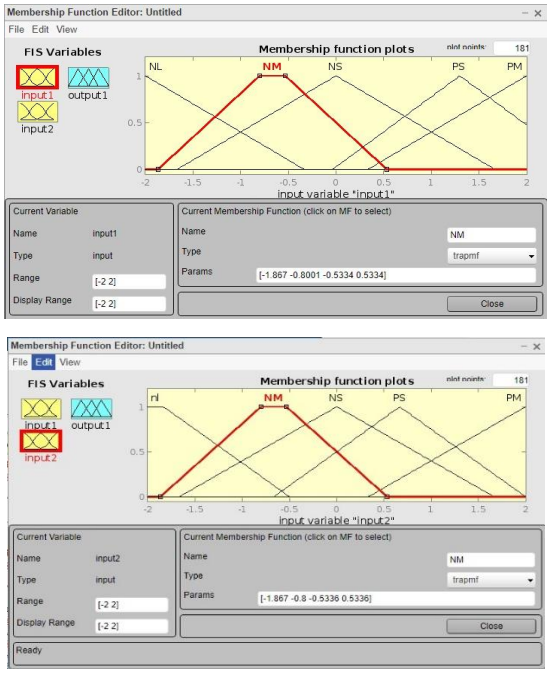

Fig. 4 – Fuzzy inputs

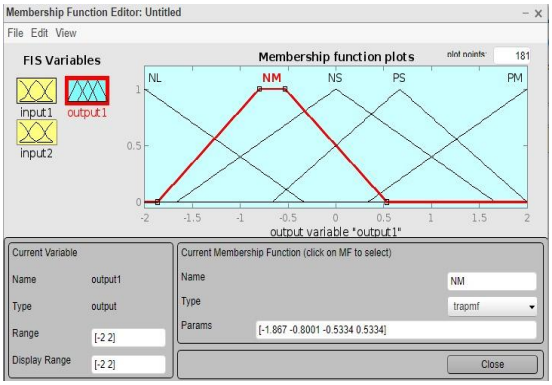

Fig. 5 – Fuzzy output

The closed loop system with a FOPID controller is then examined. The FOPID controller takes the role of the pi controller. The motor rotates at 1300 rpm, and 4 nm of torque is produced. Rise time is cut in half, from 0.6 to 0.45 seconds. There is a 2.3 to 1.4 second reduction in settling time. Peak time is modified to 0.53 seconds from 0.51 seconds, and steady state error is decreased from 6.1 to 3.2.

FLC can make use of vague knowledge. The main four elements of FLC are fuzzification, inference mechanisms (to select the appropriate rule of a given condition), and defuzzification. FLC is provided with two distinct inputs.

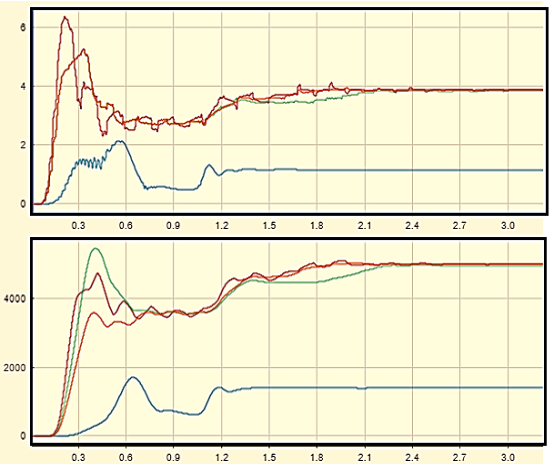

Fig. 6 – Motor speed and torque response

Fig. 4 display the input variables 1 and 2. In Fig. 5 the output variable is displayed. 1300 rpm is the motor speed graph as shown in Fig. 6. 4 nm is the torque response. Table 3 displays a comparison of the time domain parameters attained for various controller implementations.

Table 3 – Comparison of controller performances

Controller	T_r	T_s	T_p	E_{ss}
FOPID	0.35	1.4	0.43	2.8
FLC	0.3	0.6	0.46	0.08

5. EXPERIMENTAL RESULTS

The proposed converter's functionality is tested using the design parameters listed before. For the experimental verification, the voltage utilised is down by a factor of 4. The suggested converter, can drive 0.5 HP, 400 V induction motor are included in the hardware arrangement.

Bidirectional converter's LV side is powered by a 24 V DC source, which is then increased to 80 V DC on the HV side. On the HV side, a three-phase induction motor is linked as a load using an inverter.The proposed system prototype setup is shown in Fig. 7 The power converter utilised in the arrangement receives the firing pulses from the PIC micro controller PIC16F84A. As indicated in Fig. 8, 24 V is the input supply voltage taken into consideration when testing the hardware.

The switching pulses for the semiconductor switch in the proposed system are shown in Fig. 9. A 24 V input is increased to an 80 V output. Fig. 10 depicts the experimental output voltage. Three phase inverter is coupled to DC/DC converter. Fig. 11 illustrate the inverter's power output voltage.

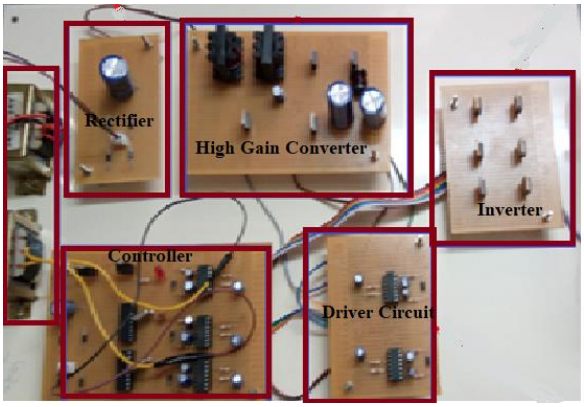

Fig. 7 – Test Bench for proposed system

Fig. 8 – Input voltage

Fig. 9 – Switching pulse for S_1 & S_2 of high gain converter

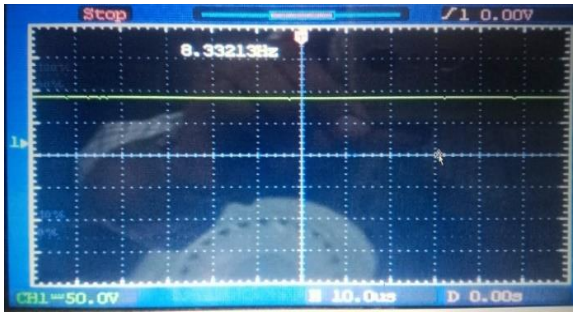

Fig. 10 – Output voltage of high gain converter

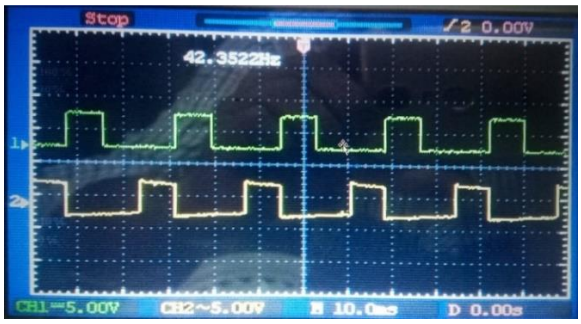

Fig. 11 – Output voltage of three phase inverter

6. CONCLUSION

Due to their widespread popularity, induction motor-fed electric vehicles (EVs) must have their speed within control. For this field, PID controllers are well known. However, it requires an advanced as well as a robust controller like FLC due to its inability to adapt to the new working state. The proposed system is therefore modelled and simulated. The outcomes of the *Z* source bidirectional DC to DC converter inverter system and the proposed system are examined. It is proven to perform more effectively than conventional Z source DC-DC converter. It is examined with a step change in load torque. With FLC, the steady state inaccuracy is decreased to 0.1 RPM and the settling time is reduced to 0.49 seconds.

REFERENCES

1. Vahid Samavatian, Ahmad Radan, *Int. J. Electr. Power Energy Syst.* **63**, 446 (2014).
2. A. Geetha, C. Subramani, T.M. Thamizh Thentral, V. Krithika, S. Usha, *J. Phys. Conf. Ser.* **1000**, 012101 (2018).
3. Yi-Ping Hsieh, Jiann-Fuh Chen, Lung-Sheng Yang, Chang-Ying Wu, Wei-Shih Liu, *IEEE Trans. Ind. Electron.* **61** No 1, 210 (2014).
4. T.F. Wu, Y.C. Chen, J.G. Yang, C.L. Kuo, *IEEE Trans. Power Electron.* **25** No 7, 1915 (2010).
5. C.-C. Huang, T.-L. Tsai, Y.-C. Hsieh, H.-J. Chiu, *Energies* **11** No 10, 2618 (2018).
6. A.K. Rathore, U.R. Prasanna, *IEEE Trans. Ind. Electron.* **60** No 10, 4482 (2013).
7. P. Xuewei, A.K. Rathore, *IEEE Trans. Ind. Electron.* **61** No 5, 2307 (2014).
8. Y. Zhang, Y. Gao, L. Zhou, M. Sumner, *IEEE Trans. Power Electron.* **33** No 11, 9459 (2018).
9. A. Ajami, H. Ardi, A. Farakhor, *IEEE Trans. Power Electron.* **30** No 8, 4255 (2015).
10. R.Y. Duan, J.D. Lee, *IET Power Electron.* **5** No 1, 115 (2012).